




Cuprizone Administration Alters the Iron Metabolism in the Mouse Model of Multiple Sclerosis

E. Varga¹ · E. Pandur¹ · H. Abrahám² · A. Horváth³ · P. Ács⁴ · S. Komoly⁴ · A. Miseta⁵ · K. Sipos^{1,6} 

Received: 31 October 2017 / Accepted: 13 February 2018 / Published online: 20 February 2018
© Springer Science+Business Media, LLC, part of Springer Nature 2018

Abstract

Cuprizone (CZ) is a widely used copper chelating agent to develop non-autoimmune animal model of multiple sclerosis, characterized by demyelination of the corpus callosum (CC) and other brain regions. The exact mechanisms of CZ action are still arguable, but it seems that the only affected cells are the mature oligodendrocytes, possibly via metabolic disturbances caused by copper deficiency. During the pathogenesis of multiple sclerosis, high amount of deposited iron can be found throughout the demyelinated areas of the brain in the form of extracellular iron deposits and intracellularly accumulated iron in microglia. In the present study, we used the accepted experimental model of 0.2% CZ-containing diet with standard iron concentration to induce demyelination in the brain of C57BL/6 mice. Our aim was to examine the changes of iron homeostasis in the CC and as a part of the systemic iron regulation, in the liver. Our data showed that CZ treatment changed the iron metabolism of both tissues; however, it had more impact on the liver. Besides the alterations in the expressions of iron storage and import proteins, we detected reduced serum iron concentration and iron stores in the liver, together with elevated hepcidin levels and feasible disturbances in the Fe–S cluster biosynthesis. Our results revealed that the CZ-containing diet influences the systemic iron metabolism in mice, particularly the iron homeostasis of the liver. This inadequate systemic iron regulation may affect the iron homeostasis of the brain, eventually indicating a relationship among CZ treatment, iron metabolism, and neurodegeneration.

Keywords Cuprizone · Multiple sclerosis · Iron metabolism · Neurodegeneration

Electronic supplementary material The online version of this article (<https://doi.org/10.1007/s10571-018-0578-5>) contains supplementary material, which is available to authorized users.

✉ K. Sipos
katalin.sipos@aok.pte.hu

- ¹ Department of Pharmaceutical Biology, Faculty of Pharmacy, University of Pécs, Rókus str. 2., Pécs 7624, Hungary
- ² Department of Medical Biology and Central Electron Microscope Laboratory, Medical School, University of Pécs, Szigeti str. 12., Pécs 7624, Hungary
- ³ Department of Neurosurgery, Medical School, University of Pécs, Rét str. 2., Pécs 7623, Hungary
- ⁴ Department of Neurology, Medical School, University of Pécs, Rét str. 2., Pécs 7623, Hungary
- ⁵ Department of Laboratory Medicine, Medical School, University of Pécs, Ifjúság str. 13., Pécs 7624, Hungary
- ⁶ Szigeti str. 12., Pécs 7624, Hungary

Introduction

Multiple sclerosis (MS) is a chronic inflammatory disease of the central nervous system (CNS), which leads to neurodegeneration. The most important characteristic features of multiple sclerosis are inflammation, primary demyelination and axonal injury, microglia activation, mitochondrial dysfunction, and chronic oxidative injury (Mahad et al. 2015). MS lesions can be categorized into four types of lesions (I–IV). Among these, pattern III lesions are distinguished by oligodendrocyte apoptosis, microglia activation, and metabolic stress (Steelman et al. 2011).

CZ is a copper chelating agent, which is widely used to induce non-autoimmune animal mouse model of MS to study the mechanisms of focal demyelination and remyelination. CZ intoxication results in demyelination of corpus callosum (CC), besides other brain regions (Denic et al. 2010). These events are very similar to those that can be found in pattern III MS lesions (Steelman et al. 2011). The accepted experimental treatment means a 0.2% CZ-containing diet

for 4–6 weeks, while chronic inflammation is minimal and complete acute demyelination occurs. This is followed by recovery on normal diet with extended remyelination (Praet et al. 2014; Kipp et al. 2009). CZ toxicity seems to affect only the mature oligodendrocytes, while other cell types in the CNS are not affected (Bénardias et al. 2013; Xu et al. 2010). There are two hypotheses present in the literature for the CZ-induced pathology: (1): Cu^{2+} deficiency and (2): Cu^{3+} chelation. It is assumed that copper deficiency is the main effect of CZ treatment, leading to various metabolic disorders of the oligodendrocytes, including mitochondrial dysfunction. However, administration of extra copper did not protect the animals or cells from the toxic effects of CZ (Denic et al. 2010; Praet et al. 2014; Gudi et al. 2014). During remyelination, oligodendrocyte precursor cells (OPCs) are activated, migrate to the lesion site, and differentiate into mature myelinating oligodendrocytes (Rawji et al. 2016). It seems that both demyelination and remyelination require the presence of macrophages and microglia cells. These cells are necessary for the clearance of myelin debris, they also store the excess of released iron during demyelination. Once remyelination occurs, they deliver iron to oligodendrocytes and help OPC maturation with the release of growth factors (Rawji et al. 2016; Olah et al. 2012). Although the neuropathological changes caused by CZ are well described, the molecular mechanisms responsible are far from understood. Some argue that CZ is unable to pass through the mouse duodenal membrane and even do not cross the neuronal plasma membrane. Therefore, it is possible that the toxic mechanism of CZ is generated by the copper-deficient diet (Benetti et al. 2010). However, besides the systemic copper deficiency, it seems that the brain is able to maintain its copper homeostasis, because no changes in the copper concentration of different brain regions are visible after CZ administration (Moldovan et al. 2015). CZ also disturbs normal hepatic function, and induces megamitochondria formation in the liver of treated mice (Praet et al. 2014; Moldovan et al. 2015).

Iron is an essential element for living organisms and involved in fundamental biological functions. In the brain, iron is needed for oxygen transportation, DNA synthesis, myelin synthesis, mitochondrial function, and neurotransmitter synthesis (Rouault and Cooperman 2006). Iron homeostasis is strictly controlled in order to maintain normal physiological functions. High levels of iron can result in iron accumulation, which can be harmful and lead to oxidative damage and cell death. In addition, it is known that chronic severe iron deficiency leads to hypomyelination both in human and animal studies (Algarín et al. 2003; Ortiz et al. 2004). Iron is highly important for myelin production as a required co-factor for cholesterol and lipid biosynthesis and oxidative metabolism of oligodendrocytes (Connor and Menzies 1996). In the brain,

iron is constantly exchanged between neurons, astrocytes, and microglia. How the different cell types acquire and release iron remains to be elucidated (Rouault and Cooperman 2006). The iron homeostasis of the CNS is a separate system by the blood–brain barrier and blood–cerebrospinal barrier, with connections to systemic iron metabolism. Blood vessels of brain interstitium and epithelial cells of the choroid plexus constitute a barrier that protects the CNS, and specific mechanisms are required for the import of nutrients. In consequence of iron depletion in the brain, iron uptake via the blood–brain barrier cells increases from the systemic circulation (Rouault 2001). Most iron can be found in oligodendrocytes and myelin particularly in the white matter, in the form of ferritin and transferrin (Ward et al. 2014; Todorich et al. 2009). Oligodendrocytes contain intracellular transferrin for the mobilization of iron and take up the majority of iron via ferritin receptors from H-ferritin provided by microglia cells (Todorich et al. 2011). This phenomenon is crucial in the white matter, which is in correlation with the profile of myelination (Williams et al. 2012). Copper is also an important co-factor for many enzymes (Williams et al. 2012). Iron and copper homeostasis in some pathways are connected to each other. The major biological links between copper and iron homeostasis are the copper-containing ferroxidases, like ceruloplasmin (Cp) and their interaction with ferroportin (Fp) for proper iron release (Lenartowicz et al. 2014; Hentze et al. 2010).

During healthy aging, iron accumulates in the brain mainly in oligodendrocytes, myelin, and microglia in non-toxic ferric form. Iron accumulation at certain brain regions shows functional relationship to myelin production (Todorich et al. 2009; Heidari et al. 2016). The amount of iron accumulated in oligodendrocytes affects the quantity and quality of the produced myelin (Ortiz et al. 2004). It has been shown that iron deficiency results in hypomyelination, and therefore, it is clear that iron is essential for the optimal function of oligodendrocytes (Algarín et al. 2003). In MS, myelin and oligodendrocytes are damaged and iron is released into the extracellular space, where it is converted to the toxic ferrous form and contributes to the increase of reactive oxygen species (ROS) in active MS lesions. Microglia and macrophages accumulate the liberated iron throughout the demyelinated area. These iron-containing microglia and macrophages undergo senescence, which also contributes to oxidative stress with the second wave of iron release. Iron is also located in axons, thus, together with the oxidative burst axonal iron accumulation may eventually lead to neurodegeneration (Mahad et al. 2015; Ward et al. 2014; Hametner et al. 2013). Furthermore, both gray and white matter regions are characterized by high iron levels in the form of extracellular deposits in animal model of MS (Williams et al. 2012).

Our aim in this study was to elucidate whether CZ administration influences iron metabolism in mice. We found that CZ had a significant impact on iron metabolism regulation in the CC of the CNS as well as in the liver. According to our results, CZ disturbs both the iron storage and mitochondrial iron–sulfur (Fe–S) cluster assembly in the liver, causing perturbations in systemic and local iron metabolism as well. Our work would contribute to better understand the mechanism of CZ action, besides shedding some light on the relationship of iron metabolism and neurodegeneration.

Materials and Methods

Animals

C57BL/6 4-week-old male mice were fed normal rodent diet containing 180 mg/kg iron for 4 weeks, before they were divided into four groups each with 7 animals. The control group (NK) remained on the original diet. Animals in the other three groups were fed with 0.2% CZ-containing food for 4 weeks. One group of CZ-treated animals (NC) was sacrificed for the experiments right after the end of CZ treatment. The rest of the animals received a diet without CZ for 2 days (NC2d) or for 2 weeks (NC2w) in order to study the early and later effects of CZ withdrawal. Animals were kept at sterile conditions and were weighed on a daily basis. Blood was drawn from the animals at the beginning of the CZ treatment and before scarification. 3 animals of each group were investigated under magnetic resonance imaging (MRI). After the experiment, 3 animals in each group were perfused and the organs were fixed for electron microscopic and immunohistochemical studies. The organs of other 3 animals from each group were removed the following way without perfusion for gene expression analysis. Mice were deeply anesthetized with a mixture of diazepam and xylazine. Skin of the animals was carefully removed from the skull, then the skull was opened along the sagittal suture. Parietal bones were removed and the brain was taken out and put in an Eppendorf tube and was snapshot frozen in dry ice. Similarly, livers were dissected from the animals, frozen, and kept at -80°C for further use.

MRI

MRI was performed on a 3T clinical scanner (Siemens TIM Trio, Erlangen, Germany) with a field gradient strength of 40 mT/m. Excitation was performed with the body coil, while a commercial loop RF coil with an inner diameter of 40 mm (Siemens Medical Solutions, Erlangen, Germany) was applied for signal detection. Each mouse was fixed in a custom-built MRI-compatible head-fixing device, with its head pulled through the loop of the RF coil. The mice were

anesthetized with intraperitoneal administration of 50 mg/kg ketamine. After the acquisition of scout images of the mouse brain, T2-weighted scans with a turbo spin echo imaging sequence (TR/TE = 3000/90 ms, slice thickness 0.8 mm, field of view (FOV) $25 \times 25 \text{ mm}^2$, matrix 128×128 , bandwidth 50 Hz/Px, number of slices 11, number of averages 5) and fluid-attenuated inversion recovery (FLAIR) scans with a turbo spin echo sequence (TR/TE/TI 6400/90/1600 ms, slice thickness 1 mm, FOV $25 \times 25 \text{ mm}^2$, matrix 128×128 , bandwidth 50 Hz/Px, number of slices 6, number of averages 2) served as structural images. T1 mapping was performed by an inversion recovery method, applying series of five turbo spin echo imaging measurements with different inversion times (TR/TE/TI 1840/27/50, 150, 400, 700, 1180 ms, slice thickness 1 mm, FOV $25 \times 25 \text{ mm}^2$, matrix 128×128 , bandwidth 50 Hz/Px, number of slices 6, number of averages 1). Two-dimensional time of flight imaging was carried out in a single slice at the level of the carotid arteries in order to determine if the animal was alive at the end of the scanning.

Image Processing

Quantitative T1 maps were calculated voxelwise by using Matlab software's curve fitting toolbox (MathWorks, Natick, MA). The signal intensities measured with different inversion times were fitted with the following equation:

$$S = |S_0 * (1 - 2 * \exp(-TI/T_1) + \exp(-TR/T_1))|,$$

where S is the signal intensity, S_0 is the signal intensity at thermal equilibrium, T_1 is the inversion time, and TR is the repetition time. T_1 values in the CC were measured by manually placing regions of interest on the CC of the mice on the T_1 map.

Fixation and Embedding of Animal Tissues

Following anesthesia, animals were transcardially perfused with phosphate buffer (PB 0.1 M, pH 7.4) followed by with 4% buffered paraformaldehyde. After removal from the skull, brains were divided with a midline cut. One hemisphere was post-fixed in the same fixative used for the perfusion for 4 h at room temperature, then dehydrated and embedded in paraffin. Blocks were coronally cut with a microtome at $10 \mu\text{m}$ and sections were mounted on gelatin-coated slides for immunohistochemistry.

The other hemisphere was cut perpendicular to its longitudinal axis at the level of the optic chiasm and 1 mm^3 large tissue blocks containing the CC at the level of the septum was prepared for electron microscopic examinations. Then tissue blocks were immersed into a fixative containing 2.5% glutaraldehyde buffered with PB for overnight at 4°C . Then blocks were fixed in 1% osmium tetroxide for 35 min and dehydrated with increasing concentration of ethanol. 70%

ethanol containing 1% uranyl acetate was used to increase contrast. After complete dehydration in ascending ethanol series concentration, blocks were transferred to propylene oxide before being placed into aluminum-foil boats and then embedded into gelatin capsule containing Durcupan resin (Sigma, Budapest, Hungary).

Immunohistochemistry

Following deparaffination, sections were rehydrated, and washed with Tris buffer (TB, 0.05 M, pH 7.6). Slides were then put in 80-mL plastic jars filled with citrate buffer (pH 6.0) and repeatedly heated in a microwave oven (Optiquick Compact, Moulinex) operating at a frequency of 2.45 GHz and 800 W power setting. After three heating cycles of 5 min each, slides were allowed to cool at room temperature and were repeatedly washed in TB. Sections were then preincubated in normal horse serum (1% in TB, Vector Laboratories, Burlingame, CA) for 1 h. This step was followed by overnight incubation of sections in the primary antibodies. Binding was visualized with biotinylated secondary antibody and with the avidin–biotin–peroxidase detection system (Universal Vectastain ABC Elite Kit, Vector Laboratories, Burlingame, CA). The chromogen was 3,3'-diaminobenzidine (DAB), and the immunoreaction was carried out under visual control. Sections were counterstained with cresyl violet, dehydrated, cleared with xylene, and covered with DePeX (Fluka, Switzerland). Control sections were treated similarly, except that the primary antiserum was omitted from the procedure. The specificity of anti-myelin basic protein (MBP) antiserum has already been determined by the company. Furthermore, if the primary antibody was omitted no immunostaining was observed. The following antibodies were used for the immunohistochemistry: mouse anti-MBP (1:100, Novocastra, New Castle upon Tyne, UK), anti-gial fibrillary acidic protein (GFAP) (DAKO, Glostrup, Denmark), and anti-Iba-1 (Merck Millipore, Budapest, Hungary) antibodies.

Densitometry

For the density measurements of MBP-immunoreactivity, digital black and white images were captured. Gray value intensity of the region of interest (ROI) and that of the background of the images were measured with ImageJ software (an open source image processing and analyzer program written in Java and supported by the NIH, USA). The values measured either in the ROIs or in the background were averaged and density values of the MBP-immunoreactivity were calculated by subtracting intensity values of ROIs from intensity values of background.

Electron Microscopy

Serial ultrathin sections were cut with Leica ultramicrotome, and mounted on mesh as well as on Collodion-coated (Parlodion, Electron Microscopy Sciences, Fort Washington, PA) single-slot copper grids. The ultrathin sections were contrasted by uranyl acetate and lead citrate, and were examined in JEOL 1200EX-II electron microscope.

RNA Isolation and Quantitative Real Time-PCR

After thawing of the frozen brains, millimeter-thick coronal sections were cut at the level of the septal nuclei, the diencephalon, as well as the cortex were carefully removed to isolate CC. CC was put in an Eppendorf tube and total RNA was isolated using the ReliaPrep RNA Tissue Mini-Prep System Kit (Promega, Madison, Wisconsin, USA). In the total RNA extracts, the (remained) DNA contamination was digested with the RQ1 RNase-free DNase (Promega, Madison, Wisconsin, USA) and the RNA was cleaned using the RNA Clean and Concentrator-5 Kit (Zymo Research, Irvine, CA, USA). From the livers, equal amounts of tissue were dissected and total RNA was isolated using the Direct-zol RNA MiniPrep Kit (Zymo Research, Irvine, CA, USA). RNA was reverse transcribed to cDNA from equal amount of total RNA using the High-Capacity cDNA Reverse Transcription Kit (Applied Biosystems, Waltham, MA, USA) and Oligo(dT)18 primer (Thermo Fisher Scientific, Waltham, MA, USA). Quantitative RT-PCR analysis was performed using specific primers for the genes of interest with the CFX96 Touch Real-Time PCR Detection System (Bio-Rad Laboratories, Hercules, CA, USA) and the iTaq Universal SYBR Green Supermix (Bio-Rad Laboratories, Hercules, CA, USA). Data were analyzed with the Bio-Rad CFX Manager 3.1 Software (Bio-Rad Laboratories, Hercules, CA, USA) and the comparative $2^{-\Delta\Delta C_t}$ (Livak) method. The expression level of the gene of interest was considered with the level of β -actin in each sample and relative expression of controls was considered as 1. Every sample was analyzed in four independent experiments.

Serum Hepcidin Measurements

Blood samples were prepared as pooled serum of the 7 animals in each group. Blood was drawn at the beginning of the experiment and at the end of the 4-week-CZ treatment. Serum mature hepcidin concentrations were determined with sandwich enzyme-linked immunosorbent assay (ELISA) specific for mouse hepcidin-25 (Abbexa Ltd., Cambridge, UK) according to the manufacturer's protocol. Concentrations were measured at 450 nm.

Serum Iron Measurements

Serum iron was determined with a Cobas c701 analyzer (Roche Diagnostics, Basel, Switzerland) using the IRON2 protocol and concentrations were gained in $\mu\text{mol/L}$.

Non-heme Iron Measurements

Non-heme iron contents of animal liver samples were measured according to the protocol of Rebouche et al. (Reimer et al. 2004) with the following modification: the samples were measured using a microplate in an Inspire multiplate reader (Perkin Elmer, Waltham, MA, USA). Standard curves were prepared in a similar way to that of the samples using FeCl_3 standards. The protein contents of liver homogenates were determined from the supernatant of the lysed tissues with DC protein assay kit (Bio-Rad Laboratories, Hercules, CA, USA) using bovine serum albumin as the standard. The iron contents of the liver samples were calculated as $\mu\text{M/mg}$ of protein content of the supernatants.

Western Blot Analysis

Frozen liver tissues (100 mg) were homogenized in 500 μL of RIPA buffer [25 mM Tris-HCl pH 7.6, 150 mM NaCl, 1% NP-40, 1% sodium deoxycholate, 0.1% SDS, Complete Mini protease inhibitor cocktail (Roche Diagnostics, Meylan, France)] using Dounce homogenizer. The homogenates were clarified by centrifugation at 12,000 rpm for 10 min at 4 °C. Protein contents of the supernatants were measured with DC Protein Assay Kit (Bio-Rad Laboratories, CA, USA). The same amount of protein from each sample was loaded onto 12 or 14% SDS-PAGE and transferred by electroblotting to nitrocellulose membranes (BioTrace NT, Pall Life Sciences, Port Washington, NY) and probed with rabbit polyclonal antibodies produced against mouse Fp, ferrochelatase (FC), mitochondrial ferritin (FTMT), and NFS-1 proteins (Novus Biologicals, Bio-Techne Corporation, Cambridge, UK). Every protein was analyzed in three independent experiments.

Statistical Analysis

Data are presented as mean \pm standard deviation (SD) throughout. Statistical analysis was performed using SPSS software. A one-way ANOVA followed by a Tukey's HSD post hoc test was used to test the significant differences between groups. Statistically significant differences between groups were defined as p values < 0.05 and are indicated in the legends of figures.

Results

Animals

To assess whether CZ had any effect on myelin synthesis, we carried out *in vivo* MRI measurements, used electron microscopy and immunohistochemical visualization of the CC of mouse brains.

MRI

Mean T1 relaxation times (\pm SD) in the CC were 695.34 ± 17.65 , 677.80 ± 8.68 , and 683.04 ± 32.52 ms after (NC), 2 days later (NC2d), and 2 weeks after (NC2w) the end of CZ treatment, respectively (Fig. 1). These values were higher than the T1 relaxation time measured in the CC of the control animal (633.30 ms).

Morphological Signs of De- and Remyelination

Electron Microscopy

In contrast to the large numbers of myelinated fibers observed in the CC of the control animals (Fig. 2a, b), myelin sheaths disappeared in the CZ-treated mice (Fig. 2c, d). The lack of myelin was detected around many axons in those animals that were sacrificed right after the CZ treatment (NC) or in those mice that were allowed to survive 2 days on normal lab chow following the CZ-containing diet (NC2d) (Fig. 2c, d).

In animals that were kept on normal diet for 2 weeks following the CZ treatment, signs of the remyelination were obvious. Accordingly, large number of myelinated axons was present in the CC (Fig. 2e, f). However, still significantly more unmyelinated axons were observed in

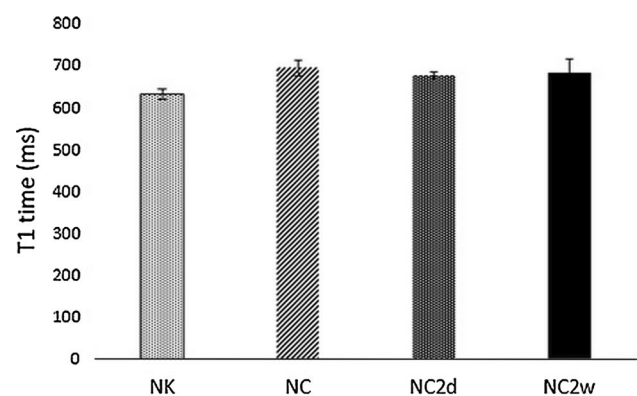
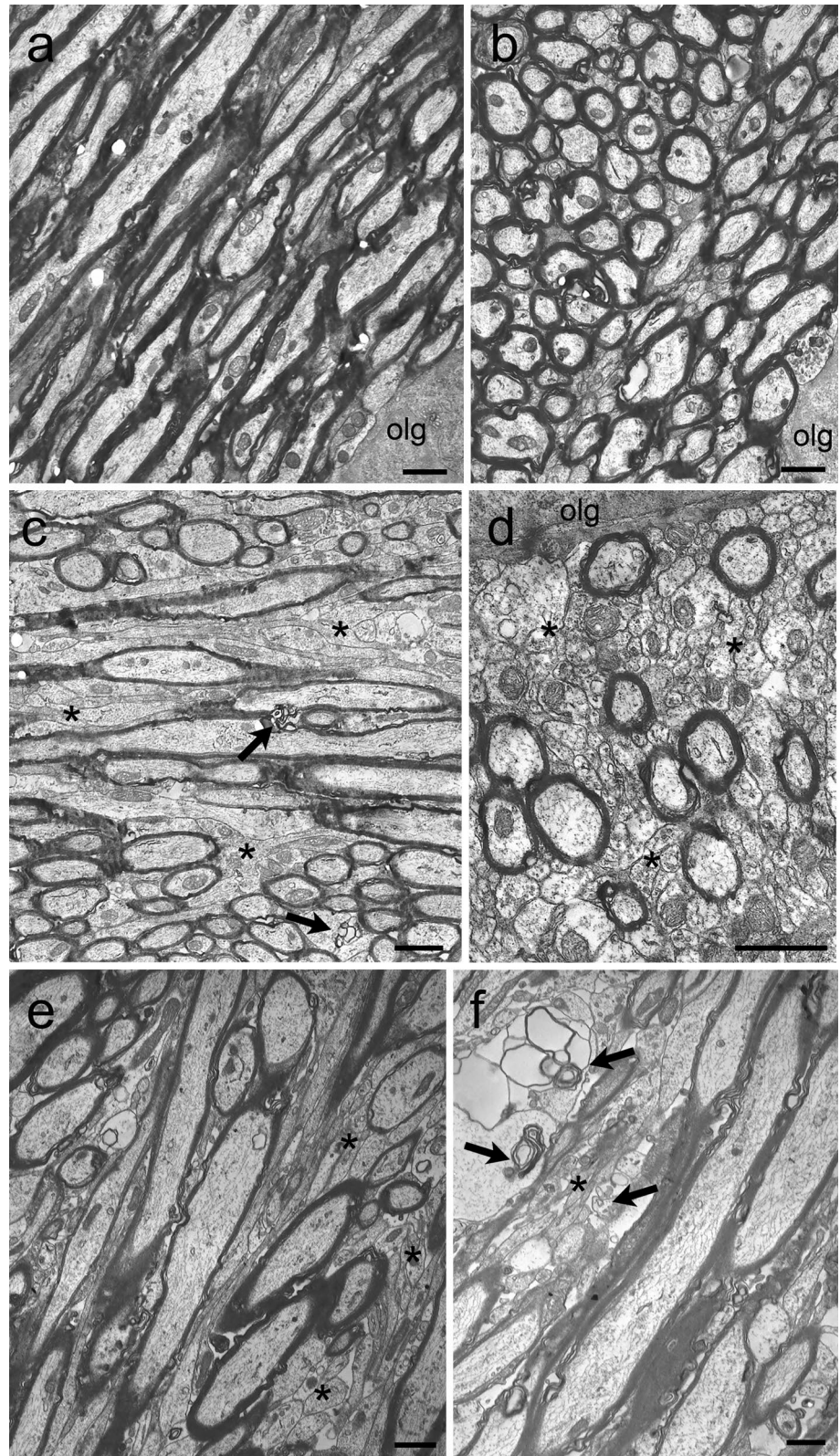


Fig. 1 Mean T1 relaxation times of the NC, NC2d, and NC2w groups after the end of CZ treatment, and control (NK) value. Whiskers indicate the standard deviation, $n = 3$ in each group

Fig. 2 Electron micrographs showing myelinated axons in the CC of a control animal (**a, b** NK), and in CZ-treated mice (**c, d** NC2d, **e, f** NC2w) in longitudinal and cross sections. Arrows point to the signs of degeneration and asterisks indicate non-myelinated axons. Scale bars: 1 μ m



these animals than in the control mice (Fig. 2a, b, e, f) indicating that remyelination was not complete. In addition, degenerating axons were also seen 2 weeks after the CZ-containing diet (Fig. 2f).

MBP Immunohistochemistry

In the brain section of the control animals, strong MBP-immunoreaction caused a homogenous brown color of the white matter tracts of CC below the neocortex (Fig. 3a). In the striatum, a large number of MBP-immunoreactive individual fibers were visible between the thick fiber tracts (Fig. 3b). Following CZ treatment, the intensity of the

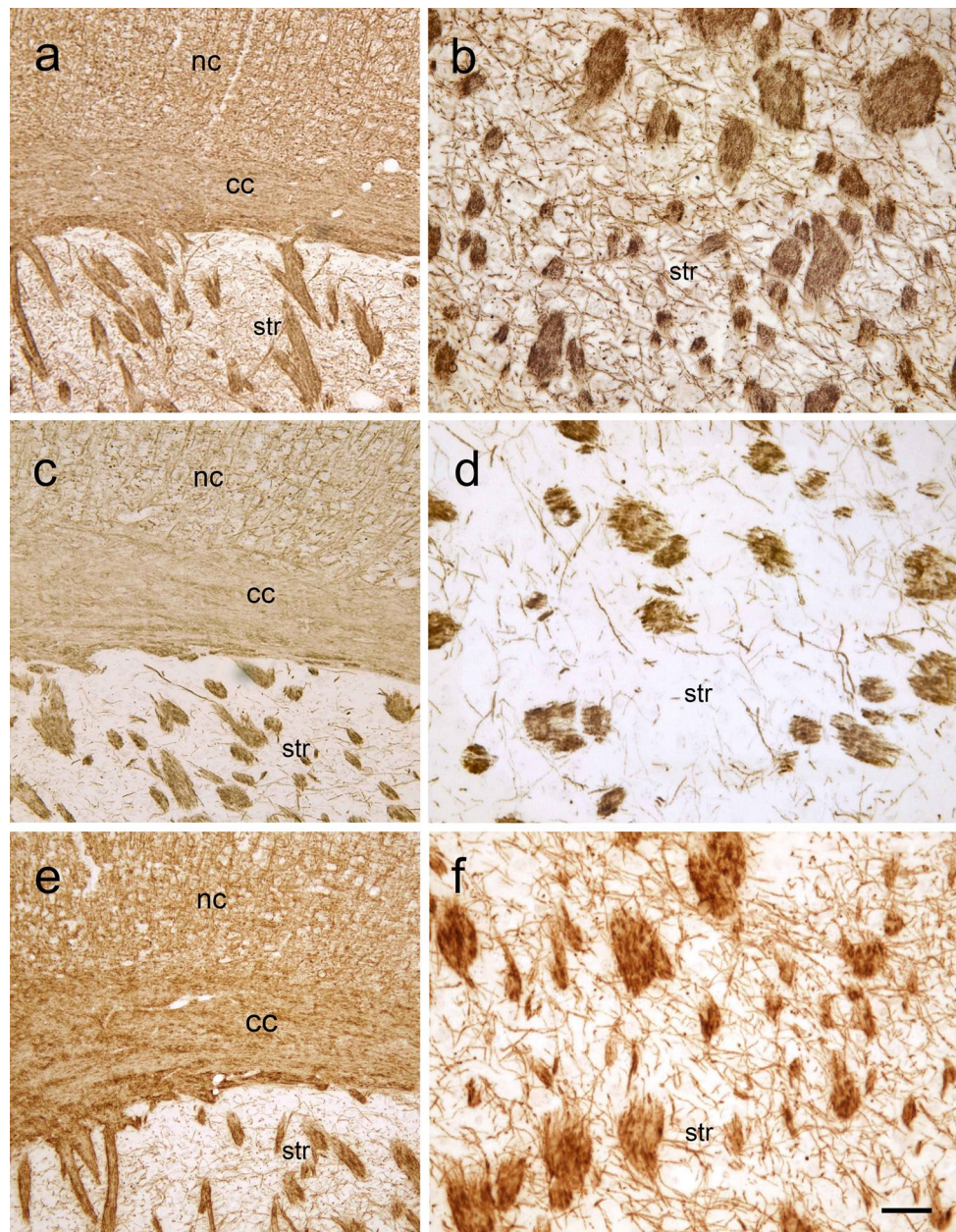


Fig. 3 MBP-immunoreaction in the CC (**a**, **c**, **e**) and in the striatum (**b**, **d**, **f**) of control (**a**, **b**) and CZ-treated mice (**c**, **f**). **a**, **b** MBP-immunoreaction in the corpus callosum (cc), in the neocortex (nc), and striatum (str) and myelinated fibers in the striatum (str) in a control mouse. **c**, **d** Weak MBP-immunoreactivity in the corpus callosum (cc) and in the striatum (str) and lower numbers of individual MBP-

immunoreactive fibers are visible in the striatum (str) in a CZ-treated mice. **e**, **f** Weakly MBP-immunoreactive fibers in the corpus callosum (cc), in the neocortex (nc) and in the striatum (str) and thin MBP-immunoreactive fibers in the striatum (str) 2 weeks after the CZ-induced demyelination. Scale bar: 50 μ m in **a**, **c**, **e** and 25 μ m in **b**, **d**, and **f**

MBP-immunoreaction decreased in the CC (Fig. 3c). In addition, markedly decreased number of individual MBP-immunoreactive fibers was detected in the striatum indicating the demyelinating effect of the CZ treatment (Fig. 3d). Measuring the optical tissue density, density of MBP-immunoreactivity was significantly reduced in the striatum following CZ treatment compared to controls. Moderate reduction of MBP-immunodensity was measured in the CC of CZ-treated animals; however, the difference was not significant (Table 1). In those animals that were kept 2 days on normal diet following the CZ treatment, MBP-immunoreactivity was visually similar to that found in those that were sacrificed right after the treatment. In the striatum, the density of the immunoreactivity was significantly reduced compared to controls (Table 1). In mice that had normal diet for 2 weeks after the CZ-containing diet, remyelination could have been detected both in the CC (Fig. 3e) and in the striatum, where the number of individual fibers between the fiber tracts increased significantly (Fig. 3f). Density of the MBP-immunoreactivity was similar both in the CC and in the striatum to the density measured in the controls (Table 1).

Reaction of Glial Cells

In control animals, lightly immunostained resting astrocytes and microglial cells were observed all over in the brain including the CC and the striatum using anti-GFAP and anti-Iba-1 antibodies (Fig. 4a, b, e, f). Following CZ treatment, mild activation of microglial cells and astrocytes was visible indicated by shorter and thicker processes and stronger GFAP and Iba-1 immunoreactivity (Fig. 4c, d, g, h). Activated glial cells were present in both the CC and the striatum.

Gene Expression Analyses

As there is relationship between copper and iron homeostasis and the function of iron in lipid metabolism is well known, we investigated the effects of CZ administration on the expression of iron homeostasis genes and some lipid metabolism genes in the CC and liver (Supplementary Table 1a, b).

Table 1 Density of the MBP-immunoreactivity in the cerebral cortex, corpus callosum, and striatum following cuprizone treatment

	Cortex	Corpus callosum	Striatum
NK	16.62 ± 5.31	22.68 ± 3.67	8.12 ± 0.05
NC	15.38 ± 4.62	17.57 ± 2.32	5.12 ± 1.34*
NC2d	16.88 ± 10.01	23.08 ± 9.318	4.94 ± 1.71*
NC2w	10.5 ± 6.25	21.3 ± 11.13	9.7 ± 2.73

Values are expressed as mean ± standard deviation. The **p* value < 0.05 was considered statistically significant, *n* = 3

Effect of CZ Treatment on Hepcidin and Ferroportin Expression in the Corpus Callosum and Liver

Corpus Callosum

The mRNA expression of HAMP, responsible for the regulation of iron release, was slightly increased following CZ treatment, but decreased to near normal value during regeneration. The expression of the main iron exporter Fp did not change following CZ treatment, which suggests that the release of iron is continuous and does not involve the action of hepcidin (Fig. 5a).

Liver

When compared to the control animals, the mRNA expression of HAMP was upregulated right after the end of the treatment, significantly decreased in the NC2d group and remained low after 2 weeks (Fig. 6b). mRNA expression and protein level of Fp remained normal, suggesting the proper iron release from the liver (Fig. 5c).

Effect of CZ Treatment on the Regulators of Hepcidin Expression

Corpus Callosum

In correlation with the increasing HAMP expression, matriptase-2 (TMPRSS6), a negative regulator of hepcidin expression, was strongly downregulated right after the end of the CZ treatment and increased significantly during remyelination. The two investigated positive regulators of HAMP expression, C/EBPα and hypoxia inducible factor 1 α (HIF1α) had the same expression level during CZ treatment as well as at the regeneration phase (Supplementary Table 1a).

Liver

The TMPRSS6 mRNA level decreased following CZ treatment and remained low during the regeneration. In the case of the positive regulators, C/EBPα and HIF1α similar changes were observed (Supplementary Table 1b). The effects of CZ on the hepcidin expression regulators are mainly different between the two tissues, CC and liver.

Effect of CZ Treatment on the Serum Hepcidin Concentration

To investigate whether the upregulation of HAMP results in the increase of hepcidin level in the blood, we measured the hepcidin concentrations of the pooled serum samples of the animals. When serum hepcidin concentrations of the

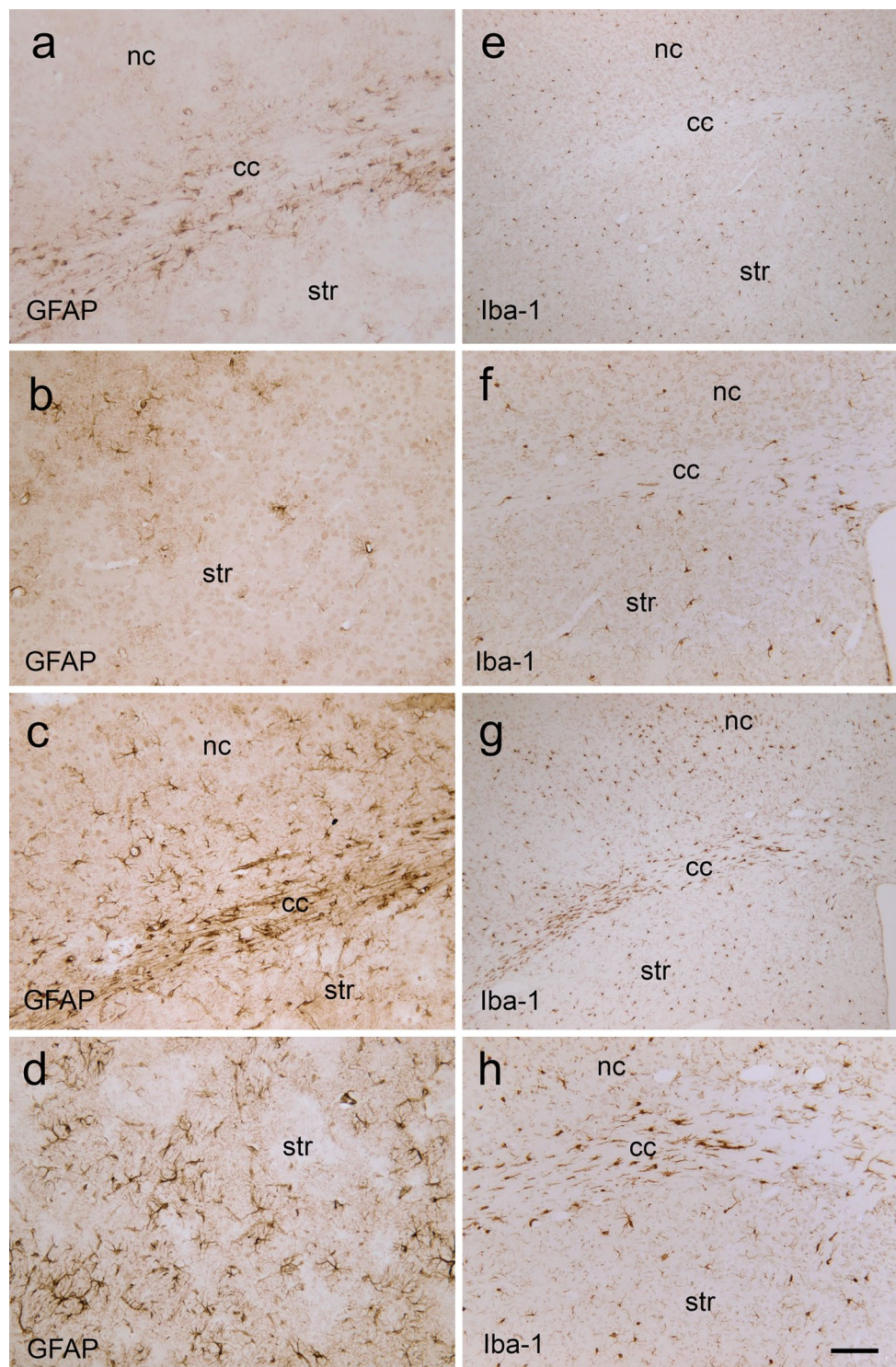


Fig. 4 GFAP and Iba-1 immunoreaction in the corpus callosum (cc), in the neocortex (nc) and in the striatum (str) in control (a, b, e, and f) and in CZ-treated mice (c, d, g, and h). Scale bar: 100 μ m in a, d, f, h and 200 μ m in e and g

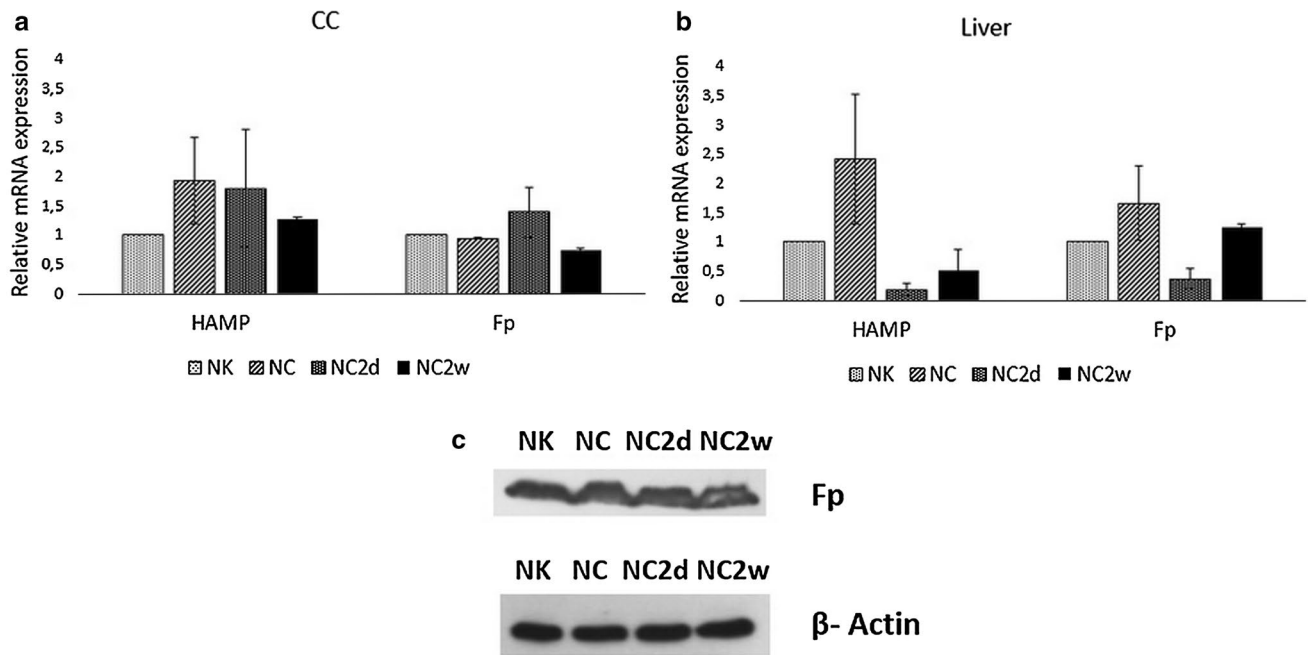


Fig. 5 **a, b** Effects of CZ treatment on the mRNA expression of HAMP and Fp in the NC, NC2d and NC2w groups compared to the NK group in the CC and liver. **c** Western blot analyses of Fp from

total protein lysates of the liver of the four experimental groups. β -actin was used as loading control. The p value < 0.05 was considered statistically significant, $n = 3$ in each group

CZ-treated animal groups were compared to the control group, there was an increase in serum hepcidin levels in the NC group. Following 2 days of regeneration, it was below the control level and started to increase again during the 2 weeks of remyelination period (Fig. 6).

Effect of CZ Treatment on the Cytosolic and Mitochondrial Iron Storage and Transport Protein Expressions in the Corpus Callosum and Liver

Corpus Callosum

When compared to the control, the expression of transferrin receptor 1 (TfR1), responsible for the import of iron into the

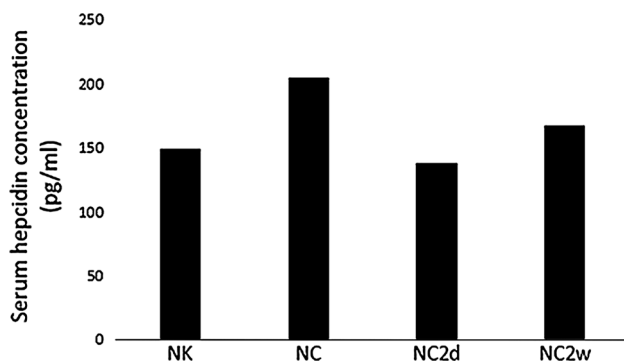


Fig. 6 Serum hepcidin concentrations of the three CZ-treated groups and control group of pooled serum samples of seven animals

cell, was unaltered in the CC. In agreement to the downregulated expression of ferritin heavy chain (FTH) after CZ treatment, there was no sign for increased cytosolic iron storage in the CC. Following CZ treatment, the mRNA expression of mitochondrial iron transport protein, mitoferrin-2 (MFRN2) was significantly increased by the end of the 2 weeks of normal diet (Fig. 7a). These results suggest that mitochondrial iron uptake becomes elevated during the remyelination. Mitochondrial ferritin (FTMT) was not detected in the CC.

Liver

TfR1 mRNA levels were markedly elevated as a result of CZ treatment in all three groups of animals. CZ treatment led to a significant reduction of the mRNA expression of FTH and light chain of ferritin (FTL) (Fig. 7b). Western blot analysis showed significantly reduced protein levels of FTH, though we found a slight increase in animals kept for 2 days on normal diet (Fig. 7e). The mRNA expression of MFRN2 was found to be significantly downregulated after the CZ treatment in the NC and NC2d groups and by the end of the regeneration period returned to normal level (Fig. 7d). The decreased mRNA level of FTMT, responsible for mitochondrial iron storage, was in correlation with the downregulated iron uptake into the mitochondrion. Unlike, when compared to the control, the protein level of FTMT in CZ-treated animals was significantly increased after the end of CZ treatment (Fig. 7f).

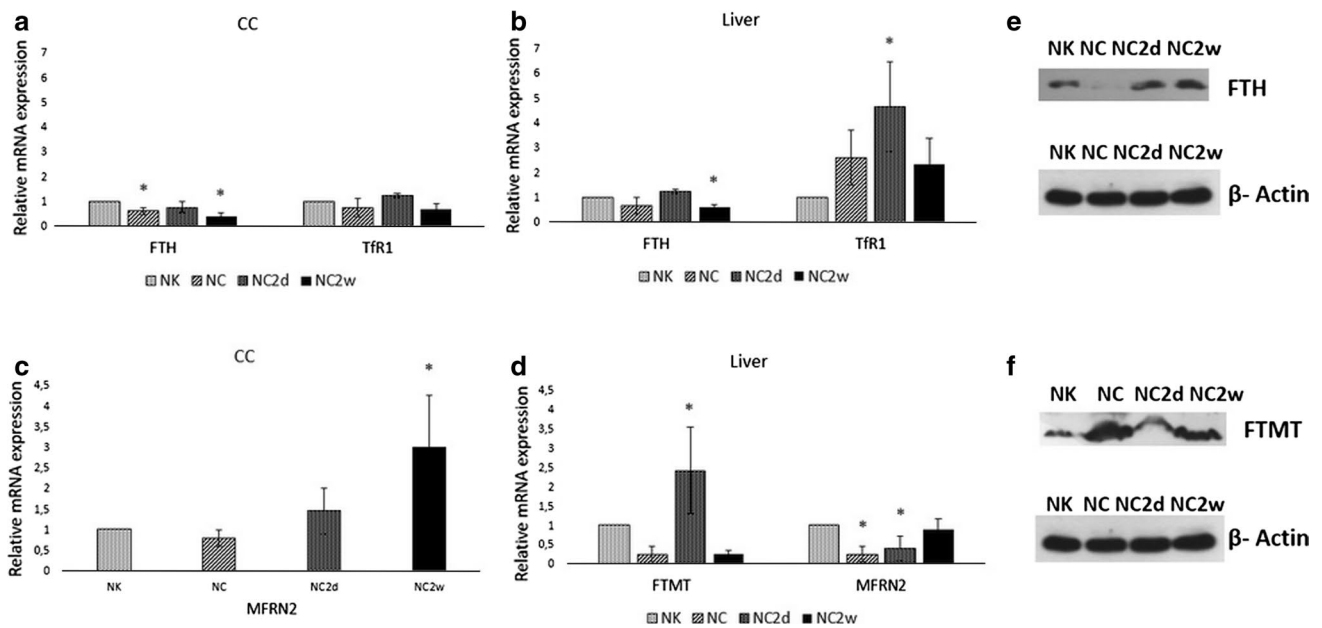


Fig. 7 Effects of CZ treatment on the investigated cytosolic and mitochondrial iron importers and iron storage proteins. **a, b** mRNA expression of FTH and TfR1 in the CC and liver. **c, d** mRNA expression of MFRN2 in the CC and liver, and FTMT in the liver in the NK, NC, NC2d, and NC2w groups compared to the NK group. In the CC,

FTMT was not detectable. **e, f** Western blot analyses of FTH and FTMT in the liver of the four experimental groups. β -actin was used as loading control. The p value < 0.05 was considered statistically significant, $n = 3$ in each group

Effect of CZ Treatment on the Expressions of Mitochondrial Iron Incorporating Proteins in the Corpus Callosum and Liver

Corpus Callosum

The expressions of NFS-1, frataxin (FRX), and Fc were found to be constant after the CZ treatment, thus, the mitochondrial Fe–S cluster and heme biosynthesis in the mitochondrion of the CC was not visibly affected; however, there was a significant reduction in the mRNA level of Fc in the NC2w group (Fig. 8a).

Liver

In the NC group, the mRNA and protein expressions of NFS-1 significantly decreased (Fig. 8b, c). The significant increase in the protein level of NFS-1 in the NC2d group might have been the result of a fast recovery (Fig. 8c). Fc, responsible for heme synthesis in the mitochondria and frataxin (FRX), important for Fe–S cluster biosynthesis were also downregulated after CZ treatment and remained at low levels during the regeneration (Fig. 8b). Following CZ treatment, there was no significant change observed in the protein level of Fc (Fig. 8c).

Non-heme Iron Content of the Liver Following CZ Treatment

The ferrozine-based iron assay was used to determine the non-heme iron content of the liver. The CZ treatment resulted in significantly decreased non-heme iron content right after the treatment in the NC group compared to control. The non-heme iron content of the liver increased during remyelination (Fig. 9).

Effect of CZ Treatment on Serum Iron Concentrations

In order to investigate whether the decreased iron content of the liver was due to the release of iron into the bloodstream, we measured the serum iron concentrations in the three experimental groups. After the end of CZ treatment, the serum iron concentrations of the animals decreased significantly and dropped further in the NC2d group. In animals that were kept on normal diet for 2 weeks following CZ treatment, serum iron concentrations started to be normalized (Fig. 10).

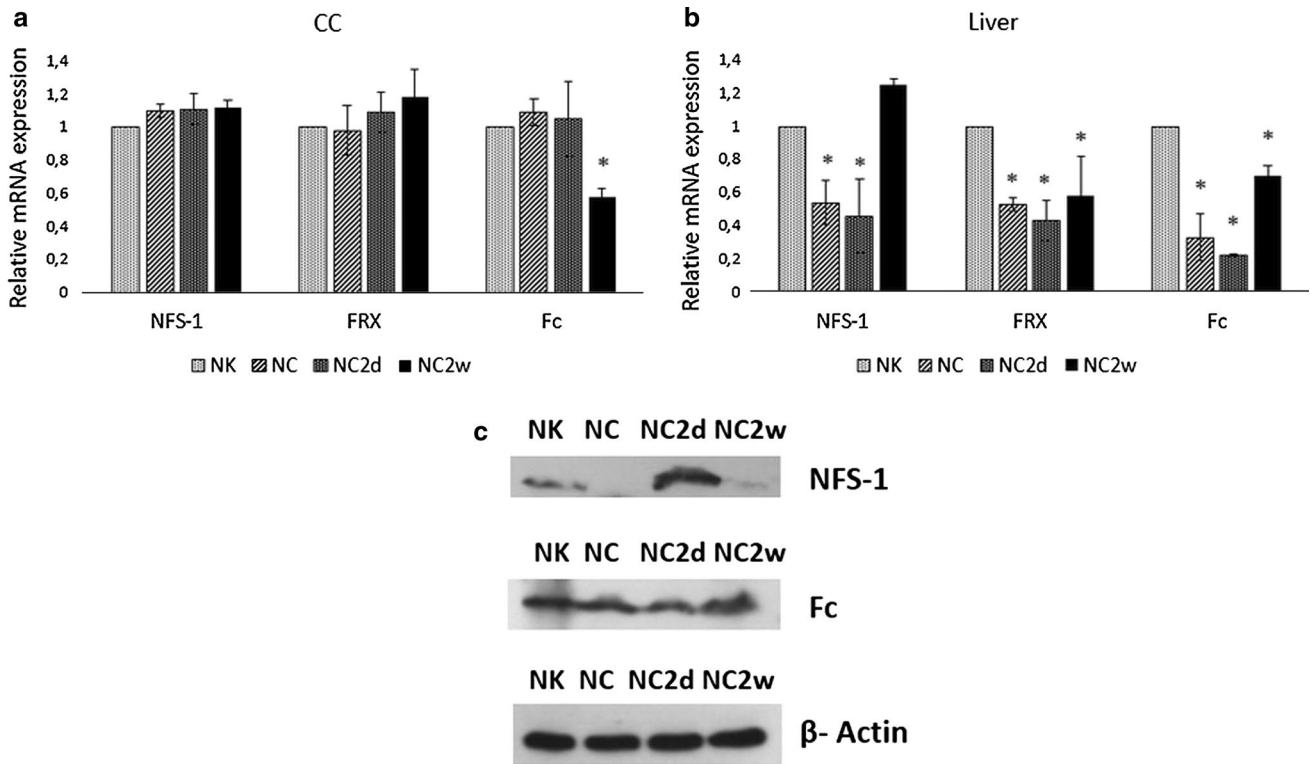


Fig. 8 Effects of CZ treatment on mitochondrial regulatory genes. **a**, **b** mRNA expression of NFS-1 and FRX and Fc in the NC, NC2d, and NC2w groups compared to the NK group in the CC and liver. **c**

Western blot analyses of NFS-1 and Fc in the liver of the four groups. β -actin was used as loading control. The p value < 0.05 was considered statistically significant, $n = 3$ in each group

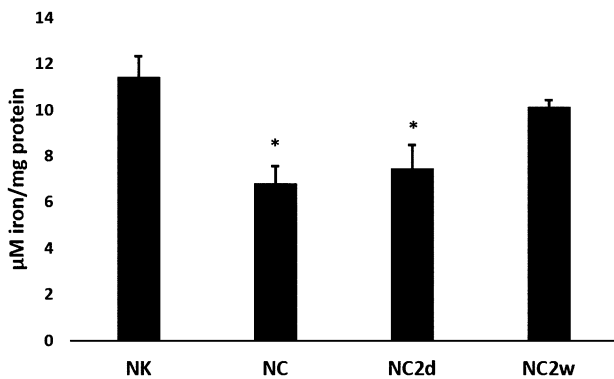


Fig. 9 Non-heme iron content of the liver in the three experimental groups, $n = 3$ in each group

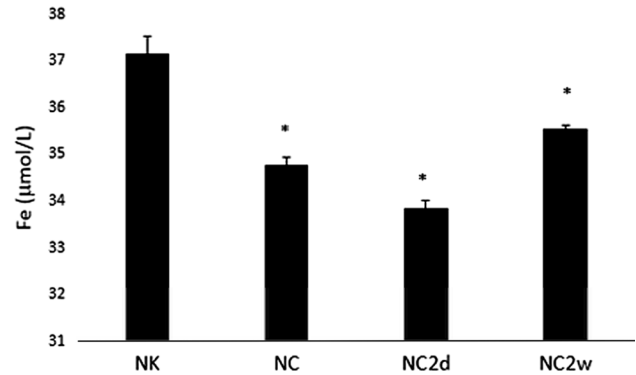


Fig. 10 Serum iron concentrations of the three groups compared to the control group. The p value < 0.05 was considered statistically significant, $n = 3$ in each group

Expression of Lipid Metabolism Genes in the Corpus Callosum and Liver Following CZ Treatment

Corpus Callosum

As the result of CZ treatment, the mRNA expression of the lipid metabolism genes, including ceramide

galactosyltransferase (Ugt8a), brain lipid-binding protein (BLBP), myelin proteolipid protein (PLP1), and MBP1 were downregulated in the CC right after the end of the CZ treatment. During the remyelination process, the expressions of these genes returned to normal level, or were upregulated. When compared to control, the mRNA level

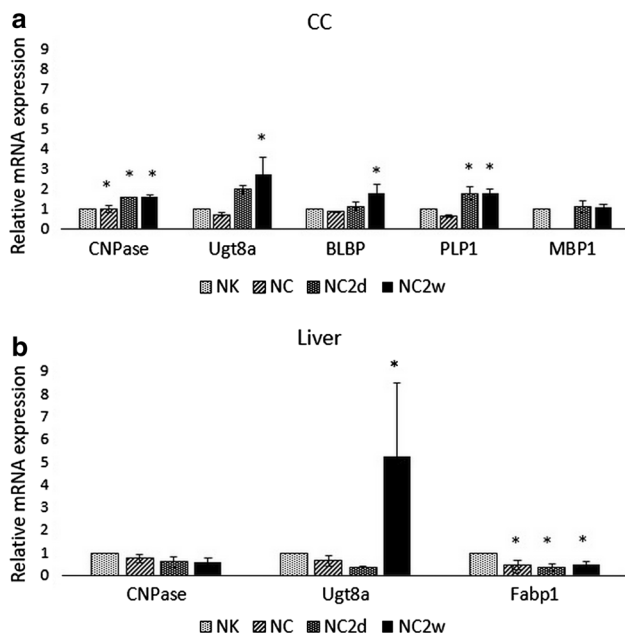


Fig. 11 Effect of CZ treatment on the expression of lipid metabolism genes in the CC and liver. **a** The mRNA expression of CNPase, Ugt8a, BLBP, PLP1, and MBP1 in the NC, NC2d, and NC2w groups compared to the NK group in the CC. **b** mRNA levels of CNPase, Ugt8a, and Fabp1 in the liver. The p value < 0.05 was considered statistically significant, $n = 3$ in each group

of 2'3'-cyclic-nucleotide 3'-phosphodiesterase (CNPase) significantly increased in all three groups. (Figure 11a).

Liver

The expressions of fatty acid binding protein 1 (Fabp1), CNPase and Ugt8a, responsible for lipid synthesis in the liver were reduced after CZ treatment, indicating disturbances in the lipid metabolism of the liver. However, the expression of Ugt8a became significantly upregulated by the end of the 2 weeks of regeneration period (Fig. 11b).

Discussion

The investigation of the pathology of CZ intoxication is well characterized and reproducible both in Swiss albino male mice and C57BL/6 mice (Steelman et al. 2011; Moldovan et al. 2015; Komoly et al. 1987). Therefore, in our study we used C57BL/6 mouse strain and took the gender and age of mice into consideration according to previous studies (Irvine and Blakemore 2006; Taylor et al. 2010; Stidworthy et al. 2003).

The CC is the most frequently investigated white matter region of the brain in the CZ-induced model of MS in mice. In addition, the majority of the changes caused by CZ

administration could be recorded in the CC (Steelman et al. 2011; Kipp et al. 2009), therefore we decided to examine the effect of CZ administration on iron homeostasis in that region of the brain. Little is known about the mechanisms of abnormal iron homeostasis in MS and how it contributes to the pathogenesis; however, iron deposits can be visible in various regions of the brain in different animal models of MS (Williams et al. 2012). In addition, the clear relationship of myelin synthesis and/or lipid metabolism and iron homeostasis (Todorich et al. 2009) gave rise to the idea of analysis of genes involved in iron uptake and release, intracellular iron storage, and iron metabolism regulation. Besides, the alterations of systemic metal homeostasis, including iron, in the CZ model of MS are also not fully understood. The liver is perhaps the most important organ in control of the iron homeostasis of the body (Ganz 2013). Since, we were interested in the systemic effects of CZ administration, the expression of genes was studied in the liver as well.

Previous results have shown (Abrahám and Lázár 2000) that following injury of the CNS, signs of mild activation of glial cells including microglial cells and astrocytes are visible as cells change their morphology during the activation process. Regarding the resting glial cells, both astrocytes and microglial cells have thin long processes, in contrast to the mildly activated cells, in which the processes are thicker and, in case of the microglial cells, shorter. In addition, activation involves the overexpression of GFAP and Iba-1, and therefore stronger GFAP-immunoreactivity and Iba-1-immunoreactivity are detected in astrocytes and microglial cells, respectively (Condorelli et al. 1990; Ito et al. 2001; Graber and Kreutzberg 1985).

Both electron microscopic and immunohistochemical preparations of the CC showed definite signs of demyelination. By the end of the CZ treatment, the myelin sheaths largely disappeared, and the lack of myelin was detected around many axons in the treated animals compared to the control group. Besides the basic morphological signs seen by electron microscopic, immunohistochemical preparations showed decreased intensity of the MBP-immunoreaction in the CC. In addition, the number of the MBP-immunoreactive fibers proved distinct decline in the striatum of the CZ-fed animals. The close morphological association between the MBP immunohistochemistry and electron microscopy presented in this work is in harmony with our earlier results (Vincze et al. 2008). These microscopic observations of demyelination support the results obtained with MRI examinations that also indicate demyelination. Moreover, our results on analyses of mRNS expression of the myelin associated genes PLP, MBP, CNPase, and Ugt8a further support the demyelination, which is also in accord with previous studies (Kipp et al. 2009; Gudi et al. 2014). CZ treatment and demyelination coincide astroglial and microglial reaction indicated by morphological changes including stronger

staining intensity (Hiremath et al. 1998). Our observations on the glial reaction further support the effectivity of the CZ treatment.

The main molecular link between iron and copper metabolism are the copper-containing ferroxidases, like Cp and hephaestin. Iron release from the cell via the iron exporter Fp and the subsequent loading onto plasma transferrin need the assistance of Cp (Hentze et al. 2010; Poli et al. 2014; Di Bella et al. 2017). To date, it is hypothesized that the pathological effects of CZ treatment may be explained partly due to copper deficiency (Denic et al. 2010; Praet et al. 2014). Incorporation of copper into apo-Cp results in the formation of the active holoenzyme (Lenartowicz et al. 2014). According to a previous study, the copper concentration of liver reduced after CZ treatment (Moldovan et al. 2015). Our data demonstrate that the expression of Cp after CZ treatment decreased in the liver and after 2 weeks of remyelination period, returned to normal level. We suppose that the downregulation of Cp was due to the copper deficiency and reduced copper concentration in the liver caused by CZ administration. In the same study mentioned above, different brain regions did not show any significant alteration in copper concentrations as a result of CZ intoxication (Moldovan et al. 2015; Jeyasingham et al. 1998). Likewise, we found no change in the expression of Cp in the CC after CZ treatment. These data suggest that the brain is able to maintain its copper homeostasis despite the obvious systemic copper deficiency.

Hepcidin plays a major role in the regulation of iron metabolism by binding to the iron exporter Fp and causing the internalization of the receptor in response to increased iron levels (Hentze et al. 2010; Rishi et al. 2015). According to our study, as a result of CZ treatment, hepcidin expression increased in the NC group of both the CC and liver, which was not followed by changes in Fp expression in the investigated tissues. However, after 2 days of remyelination time, HAMP expression was significantly downregulated in the liver, and there were no alteration in Fp protein levels in the two regenerating groups. It was demonstrated earlier that increased hepcidin treatment leads to Fp degradation in mouse hepatocytes, which indicates the role of hepcidin in regulating Fp protein stability in the hepatocytes (Ramey et al. 2010) and macrophages (Zohn et al. 2007) *in vitro*. The exact mechanism, how hepcidin regulates ferroportin degradation *in vivo*, is still unclear; however, the loss of Fp was confirmed in mouse tissues (Ward and Kaplan 2012). Our results may prove that hepcidin did not act locally on its receptor. In addition to the changes of HAMP expression following CZ treatment, similar alterations were observed in the serum hepcidin levels during the investigated period. It is possible that hepcidin is transported from the liver and has an effect on other organs. Moreover, in correlation with

the increased HAMP expression, the negative regulator of hepcidin levels, TMPRSS6 (Sangkhae and Nemeth 2017) was downregulated in both investigated tissues which seems to be the major cause of hepcidin elevation.

We were interested in the effect of CZ treatment on the iron transport and storage proteins of CC and liver. TfR1 is responsible for the uptake of iron in the form of transferrin-Fe₂, while MFRN2 can be found in the mitochondrial membrane and important for mitochondrial iron uptake. In the cytoplasm, iron is stored in ferritin heteropolymers, which provide an iron store for the mobilization of iron and lock up excess iron. In the mitochondria, iron is stored in FTMT in order to protect the organelle against iron-mediated toxicity (Hentze et al. 2010). According to our results, the import of iron into the cell via TfR1 in the CC was not significantly altered. In the liver, TfR1 expression was upregulated, although there was no visible sign of cytosolic iron storage, because the protein level of FTH decreased following CZ treatment. Iron uptake into the mitochondrion via MFRN2 was downregulated both in the CC and liver after the end of the treatment, but gradually upregulated or returned to normal levels during remyelination. Our results show an upregulation of FTMT in the liver following CZ treatment, but a decrease after 2 days of regeneration. In the CC, we cannot detect FTMT. These results indicate reduced mitochondrial iron uptake in the investigated tissues right after CZ treatment, but with an assumable mitochondrial iron storage in the liver.

As already shown, CZ induces megamitochondria formation both in oligodendrocytes and hepatocytes and disturbances in mitochondrial function, therefore it is speculated that the neurotoxic effect is in part due to the disruption of normal roles of mitochondria (Praet et al. 2014; Kipp et al. 2009). One of the key processes of normal mitochondrial function is the Fe–S cluster assembly. Fe–S clusters have crucial role in mitochondrial respiration, in the citric acid cycle, DNA metabolism, and apoptosis (Stiban et al. 2016). Another mitochondrial enzyme, Fc is the Fe–S cluster containing terminal enzyme in the heme biosynthetic pathway and catalyzes the insertion of iron into protoporphyrin IX to form heme (Crooks et al. 2010). In order to investigate the disturbances of mitochondrial iron homeostasis after CZ administration, we studied the gene expression alterations of certain mitochondrial iron-incorporating and iron-containing proteins. Under normal Fe–S cluster assembly, sulfur is provided by NFS-1 and iron is most likely provided by the protein FRX (Stiban et al. 2016). Our findings show that CZ treatment did not affect the expressions of NFS-1, FRX, and Fc in the CC. In contrast, in the liver we found intense reduction in the expression of NFS-1 and FRX after the treatment, which started to recover during the remyelination. This implies that CZ intoxication strongly affects the mitochondrial Fe–S cluster biosynthesis in the

liver, therefore the normal function of mitochondria. This might suggest disturbances of mitochondrial iron homeostasis of the liver, together with the downregulation of mitochondrial iron import proteins. In addition, the perturbation of the Fe–S cluster metabolism would increase cellular iron uptake via TfR1 and diminishes iron storage by ferritin (Galy et al. 2010). Taken together, we suggest that the decrease of cytosolic iron storage by FTH and the upregulation of iron import via TfR1 are due to the disturbance in the mitochondrial Fe–S cluster assembly. It appears that this assumable systemic turnover of mitochondrial iron homeostasis does not affect severely the CC, possibly due to the mostly autonomous regulation of iron homeostasis of the brain (Rouault and Cooperman 2006; Rouault 2001). It is known that the Fe–S cluster of Fc does not participate in catalyzing the terminal reaction of heme synthesis. Nevertheless, data suggest that impaired Fe–S cluster assembly causes reduced Fc levels (Crooks et al. 2010). Moreover, according to others, the loss of functional FRX alters heme synthesis, because FRX may provide iron for the last step catalyzed by Fc. In contrast, patients with FRX deficiency do not show significant anemia, suggesting that FRX is not essential for heme synthesis (Ye and Rouault 2010). It was shown that in iron depleted and diminished Fe–S cluster synthesis conditions, the mature Fc protein was not susceptible to degradation. However, these circumstances affect the maturation and stabilization of apo-Fc (Crooks et al. 2010). According to our results, albeit the mitochondrial iron–sulfur synthesis seems to be diminished, the Fc protein levels were not influenced. Since, the observed iron store in the form of FTMT after CZ treatment may be utilized for heme synthesis via mature Fc proteins.

We measured the non-heme iron content of the liver in the three experimental groups. Our results show a decrease in the iron content right after the end of the treatment, which started to normalize during the regeneration period. This was in correlation with the downregulated expression of FTH. We speculated that the decreased iron content of the liver was due to the release of iron into the bloodstream. However, our data demonstrated significant decrease in the serum iron concentrations as the result of CZ treatment. Other authors showed that, after CZ administration, there is no change in the iron concentration of the blood and the iron content in the liver significantly increases (Moldovan et al. 2015). Conflicting results might be due to the different time durations of CZ administration and the different methods used for iron measurements. According to our results, we assume that the observed decrease in serum iron concentration and reduced iron stores in the liver were due to suppressed iron absorption, together with high serum hepcidin levels. These conditions probably resulted from the defect of the *TMPRSS6* gene expression caused by CZ treatment,

similarly to iron refractory iron deficiency anemia (De Falco et al. 2013; Finberg 2009).

According to previous studies, the mRNA expression of myelin-associated protein genes, such as PLP, MBP, CNPase, and *Ugt8a* is dramatically downregulated already after 1 week of CZ administration and further declined after 3 weeks (Kipp et al. 2009; Gudi et al. 2014). Our results are in agreement with these observations. The mRNA expressions of the investigated lipid metabolism genes and myelin protein genes were downregulated after CZ treatment in the CC and during the remyelination period returned to normal levels. It is known that the peak period of iron uptake in the CNS coincides with the peak of myelination during development (Connor and Menzies 1996). This also suggests a close relationship between iron metabolism and myelin synthesis and the oligodendrocytes' large need for iron for optimal energy metabolism. Others described that there is no change in the iron content of cerebellum, cortex, or thalamus of CZ-fed mice (Moldovan et al. 2015). In spite, different brain regions might display different dynamics of demyelination and remyelination (Gudi et al. 2009), consequently further investigation is needed. It has been documented that conditions, such as iron deficiency, may reduce iron uptake of the brain—therefore the iron acquisition of oligodendrocytes (Connor and Menzies 1996)—which can be the reason of their metabolic disturbances. Since in our study CZ treatment resulted in decreased serum iron concentrations, the availability of iron for the brain decreased, hence the iron uptake of oligodendrocytes may have been reduced. According to recent knowledge, the iron metabolism in the CNS is a separated system but has relation to systemic iron metabolism (Rouault 2001). We hypothesize that CZ treatment affects the iron regulation of the brain, possibly via the disturbed systemic iron homeostasis, which probably cannot be normalized by the local iron metabolism regulation of the CNS. Our results suggest that beside the unique effects of CZ on myelin synthesis, CZ has a role in the dysregulation of systemic iron metabolism.

Acknowledgements The project has been supported by the Social Renewal Operational Programme [TÁMOP-4.2.2.A-11/1/KONV-2012-0017], the Economic Development and Innovation Operational Programme [GINOP-2.3.2-15], and the European Union, co-financed by the European Social Fund [EFOP-3.6.1-16-2016-0004].

Author Contributions K. Sipos, S. Komoly designed the concept of the work. E. Varga and E. Pandur performed the gene expression analysis experiments. H. Abrahám performed the electron microscopy and immunohistochemistry experiments. A. Horváth carried out the MRI measurements. P. Ács and A. Míseta participated in data analysis and interpretation. All authors helped to draft and revise the manuscript.

Compliance with Ethical Standards

Conflict of interest The authors declare that they have no conflict of interest.

Ethical Approval All applicable international, national, and/or institutional guidelines for the care and use of animals were followed. Animals were maintained under SPF conditions under permits BAI/01/1390-003/2013 (issued by the Baranya County Government Office) and SF/688-18/2013 and SF/27-1/2014 (issued by the Ministry of Agriculture).

References

- Abrahám H, Lázár G (2000) Early microglial reaction following mild forebrain ischemia induced by common carotid artery occlusion in rats. *Brain Res* 862(1–2):63–73
- Algarín C, Peirani P, Garrido M, Pizarro F, Lozoff B (2003) Iron deficiency anemia in infancy: long-lasting effects on auditory and visual system functioning. *Pediatr Res* 53(2):217–223
- Bénardias K, Kotsiari A, Skuljec J, Koutsoudaki PN, Gudi V, Singh V, Vulinovic F, Skripuletz T (2013) Cuprizone [bis(cyclohexylidenehydrazide)] is selectively toxic for mature oligodendrocytes. *Neurotox Res* 24(2):244–250
- Benetti F, Ventura M, Salmini B et al (2010) Cuprizone neurotoxicity, copper deficiency and neurodegeneration. *Neurotoxicology* 31(5):509–517
- Condorelli DF, Dell’Albani P, Kaczmarek L et al (1990) Glial fibrillary acidic protein messenger RNA and glutamine synthetase activity after nervous system injury. *J Neurosci Res* 26(2):251–257
- Connor JR, Menzies SL (1996) Relationship of iron to oligodendrocytes and myelination. *Glia* 17(2):83–93
- Crooks DR, Ghosh MC, Haller RG, Tong WH, Rouault TA (2010) Posttranslational stability of the heme biosynthetic enzyme ferrochelatase is dependent on iron availability and intact iron–sulfur cluster assembly machinery. *Blood* 115(4):860–869
- De Falco L, Sanchez M, Silvestri L et al (2013) Iron refractory iron deficiency anemia. *Haematologica* 98(6):845–853
- Denic A, Johnson AJ, Bieber AJ, Waarrington AE, Rodriguez M, Pirko I (2010) The relevance of animal models in multiple sclerosis research. *Pathophysiology* 18(1):21–29
- Di Bella LM, Alampi R, Biundo F, Toscano G, Felice MR (2017) Copper chelation and interleukin-6 proinflammatory cytokine effects on expression of different proteins involved in iron metabolism in HepG2 cell line. *BMC Biochem* 18(1):1
- Finberg KE (2009) Iron-refractory iron deficiency anemia. *Semin Hematol* 46(4):378–386
- Galy B, Ferring-Appel D, Sauer SW et al (2010) Iron regulatory proteins secure mitochondrial iron sufficiency and function. *Cell Metab* 12(2):194–201
- Ganz T (2013) Systemic iron homeostasis. *Physiol Rev* 93(4):1721–1741
- Graber MB, Kreutzberg GW (1985) Immuno gold staining (IGS) for electron microscopical demonstration of glial fibrillary acidic (GFA) protein in LR white embedded tissue. *Histochemistry* 83(6):497–500
- Gudi V, Khiabani-Moharreh D, Skripuletz T et al (2009) Regional differences between grey and white matter in cuprizone induced demyelination. *Brain Res* 1283:127–138
- Gudi V, Gingele S, Skripuletz T, Stangel M (2014) Glial response during cuprizone-induced de- and remyelination in the CNS: lessons learned. *Front Cell Neurosci* 8:73
- Hametner S, Wimmer I, Haider L, Pfeifenbring S, Brück W, Lassmann H (2013) Iron and neurodegeneration in the multiple sclerosis brain. *Ann Neurol* 74(6):848–861
- Heidari M, Gerami SH, Bassett B et al (2016) Pathological relationships involving iron and myelin may constitute a shared mechanism linking various rare and common brain diseases. *Rare Dis* 4(1):e1198458
- Hentze MW, Muckenthaler MU, Galy B, Camaschella C (2010) Two to tango: regulation of Mammalian iron metabolism. *Cell* 142(1):24–38
- Hiremath MM, Saito Y, Knapp GW, Ting JP, Suzuki K, Matsushima GK (1998) Microglial/macrophage accumulation during cuprizone-induced demyelination in C57BL/6 mice. *J Neuroimmunol* 92(1–2):38–49
- Irvine AK, Blakemore WF (2006) Age increases axon loss associated with primary demyelination in cuprizone-induced demyelination in C57BL/6 mice. *J Neuroimmunol* 175(1–2):69–76
- Ito D, Tanaka K, Suzuki S, Dembo T, Fukuuchi Y (2001) Enhanced expression of Iba1, ionized calcium-binding adapter molecule 1, after transient focal cerebral ischemia in rat brain. *Stroke* 32(5):1208–1215
- Jeyasingham MD, Rooprai HK, Dexter D, Pratt OE, Komoly S (1998) Zinc supplementation does not prevent cuprizone toxicity in the brain of mice. *Neurosci Res Commun* 22(3):181–187
- Kipp M, Clarner T, Dang J, Copray S, Beyer C (2009) The cuprizone animal model: new insights into an old story. *Acta Neuropathol* 118(6):723–736
- Komoly S, Jeyasingham MD, Pratt OE, Lantos PL (1987) Decrease in oligodendrocyte carbonic anhydrase activity preceding myelin degeneration in cuprizone induced demyelination. *J Neurol Sci* 79(1–2):141–148
- Lenartowicz M, Starzynski RR, Krzeptowski W et al (2014) Haemolysis and perturbations in the systemic iron metabolism of suckling, copper-deficient mosaic mutant mice: an animal model of menkes disease. *PLoS ONE* 9(9):e107641
- Mahad DH, Trapp BD, Lassmann H (2015) Pathological mechanisms in progressive multiple sclerosis. *Lancet Neurol* 14(2):183–193
- Moldovan N, Al-Ebraheem A, Lobo L, Park R, Farquharson MJ, Bock NA (2015) Altered transition metal homeostasis in the cuprizone model of demyelination. *Neurotoxicology* 48:1–8
- Olah M, Amor S, Brouwer N, Vinet J, Eggen B, Biber K, Boddeke HW (2012) Identification of a microglia phenotype supportive of remyelination. *Glia* 60(2):306–321
- Ortiz E, Pasquini JM, Thompson K, Felt B, Butkus G, Beard J, Connor JR (2004) Effect of manipulation of iron storage, transport, or availability on myelin composition and brain iron content in three different animal models. *J Neurosci Res* 77(5):681–689
- Poli M, Asperti M, Ruzzenenti P, Regoni M, Arosio P (2014) Hepcidin antagonists for potential treatments of disorders with hepcidin excess. *Front Pharmacol* 5:86
- Praet J, Guglielmetti C, Berneman Z, Van der Linden A, Ponsaerts P (2014) Cellular and molecular neuropathology of the cuprizone mouse model: clinical relevance of multiple sclerosis. *Neurosci Biobehav Rev* 47:485–505
- Ramey G, Deschemin JC, Durel B, Canonne-Hergaux F, Nicolas G, Vaultant S (2010) Hepcidin targets ferroportin for degradation in hepatocytes. *Haematologica* 95(3):501–504
- Rawji KS, Mishra MK, Yong VW (2016) Regenerative capacity of macrophages for remyelination. *Front Cell Dev Biol* 4:47
- Reimer J, Hoepken HH, Czerwinska H, Robinson SR, Dringen R (2004) Colorimetric ferrozine-based assay for the quantitation of iron in cultured cells. *Anal Biochem* 331(2):370–375
- Rishi G, Wallace DF, Subramaniam VN (2015) Hepcidin: regulation of the master iron regulator. *Biosci Rep* 35(3):e00192
- Rouault TA (2001) Systemic iron metabolism: a review and implications for brain iron metabolism. *Pediatr Neurol* 25(2):130–137

- Rouault TA, Cooperman S (2006) Brain iron metabolism. *Semin Pediatr Neurol* 13(3):142–148
- Sangkhae V, Nemeth E (2017) Regulation of the iron homeostatic hormone hepcidin. *Adv Nutr* 8(1):126–136
- Steelman AJ, Thompson JP, Li J (2011) Demyelination and remyelination in anatomically distinct regions of the corpus callosum following cuprizone intoxication. *Neurosci Res* 72(1):32–42
- Stiban J, So M, Kaguni LS (2016) Iron-sulfur clusters in mitochondrial metabolism: multifaceted roles of a simple cofactor. *Biochemistry* 81(10):1066–1080
- Stidworthy MF, Genoud S, Suter U, Mantei N, Franklin RJ (2003) Quantifying the early stages of remyelination following cuprizone-induced demyelination. *Brain Pathol* 13(3):329–339
- Taylor LC, Gilmore W, Ting JP, Matsushima GK (2010) Cuprizone induces similar demyelination in male and female C57BL/6 mice and results in disruption of the estrous cycle. *J Neurosci Res* 88(2):391–402
- Todorich B, Pasquini JM, Garcia CI, Paez PM, Connor JR (2009) Oligodendrocytes and myelination: the role of iron. *Glia* 57(5):467–478
- Todorich B, Zhang X, Connor JR (2011) H-ferritin is the major source of iron for oligodendrocytes. *Glia* 59(6):927–935
- Vincze A, Mázló M, Seress L, Komoly S, Abrahám H (2008) A correlative light and electron microscopic study of postnatal myelination in the murine corpus callosum. *Int J Dev Neurosci* 26(6):575–584
- Ward DM, Kaplan J (1823) Ferroportin-mediated iron transport: expression and regulation. *Biochim Biophys Acta* 9:1426–1433
- Ward RJ, Zucca FA, Duyn JH, Crichton RR, Zecca L (2014) The role of iron in brain ageing and neurodegenerative disorders. *Lancet Neurol* 13(10):1045–1060
- Williams R, Buchheit CL, Beman NE, LeVine SM (2012) Pathogenic implications of iron accumulation in multiple sclerosis. *J Neurochem* 120(1):7–25
- Xu H, Yang HJ, McConomy B, Browning R, Li XM (2010) Behavioral and neurobiological changes in C57BL/6 mice exposed to cuprizone. *Front Behav Neurosci* 4:8
- Ye H, Rouault TA (2010) Erythropoiesis and iron sulfur cluster biogenesis. *Adv Hematol* 2010:329394
- Zohn IE, De Domenico I, Pollock A et al (2007) The flatiron mutation in mouse ferroportin acts as a dominant negative to cause ferroportin disease. *Blood* 109(10):4174–4180